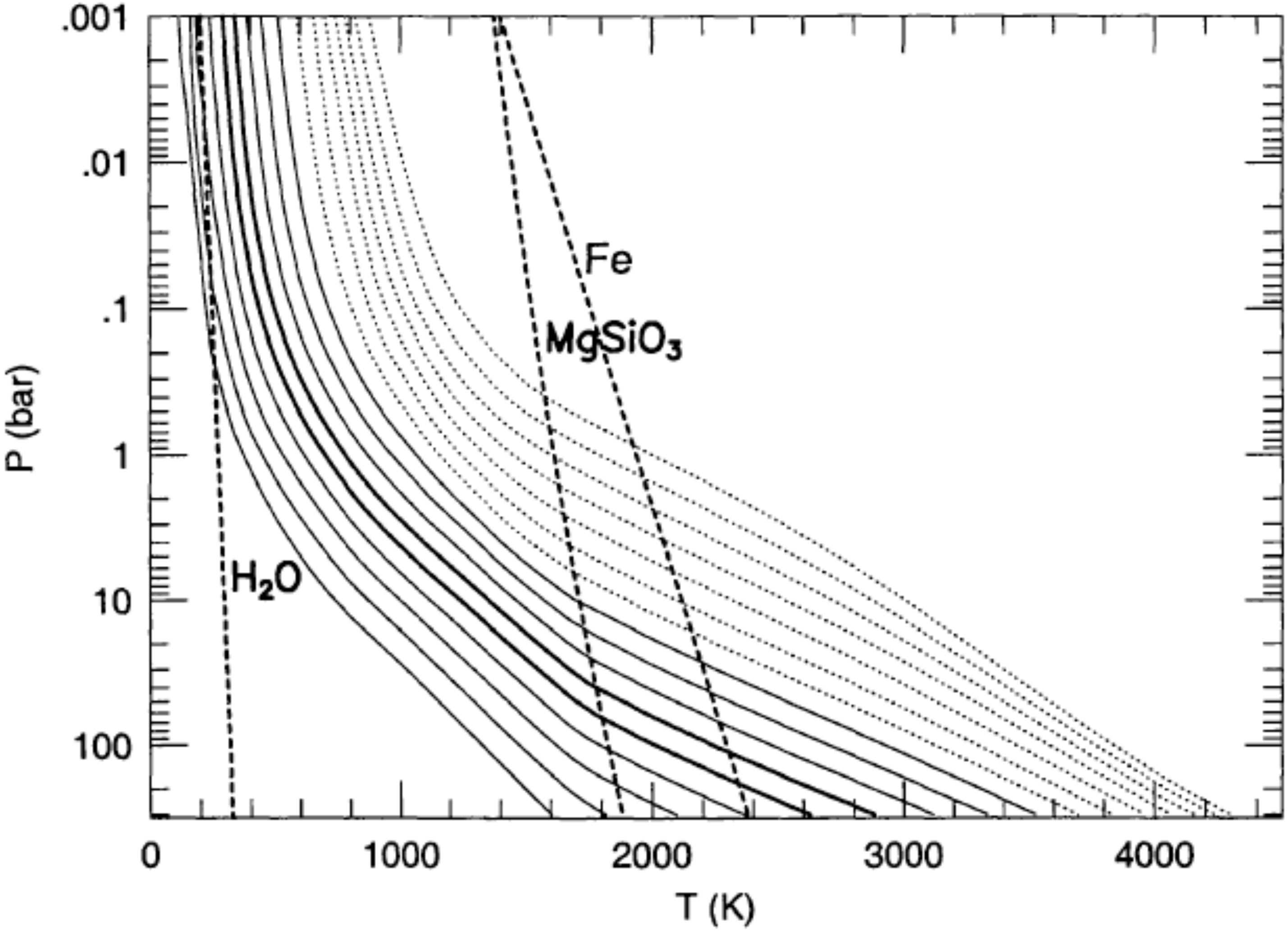

Figure 1. Model cloud-free temperature profiles for $\sim 35\,\mathrm{M_J}$ brown dwarf ($g = 10^5\,\mathrm{cm\,sec^{-2}}$) over the range $500 \leq T_{\rm eff} \leq 2000\,\mathrm{K}$ in steps of 100 K. Solid and dashed lines denote the approximate $T_{\rm eff}$ range for the

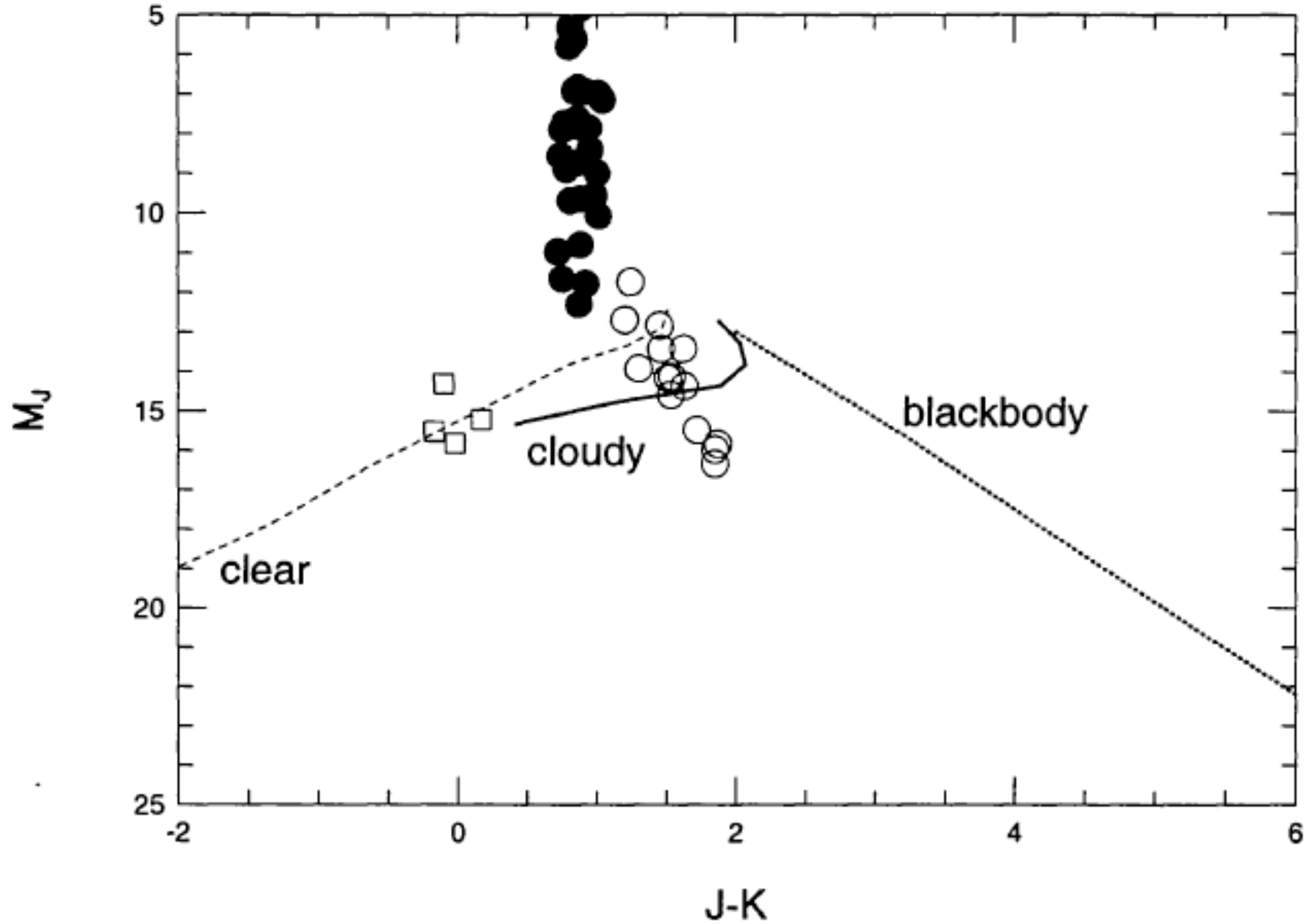

Figure 2. J vs. $J - K$ color-magnitude diagram. Filled circles represent M-dwarfs (Leggett et al. 2000), open circles denote absolute L-dwarf magnitudes (Dahn et al. this volume), and open squares denote T-dwarfs (Leggett et al. 1999; Burgasser et al. 1999). Note

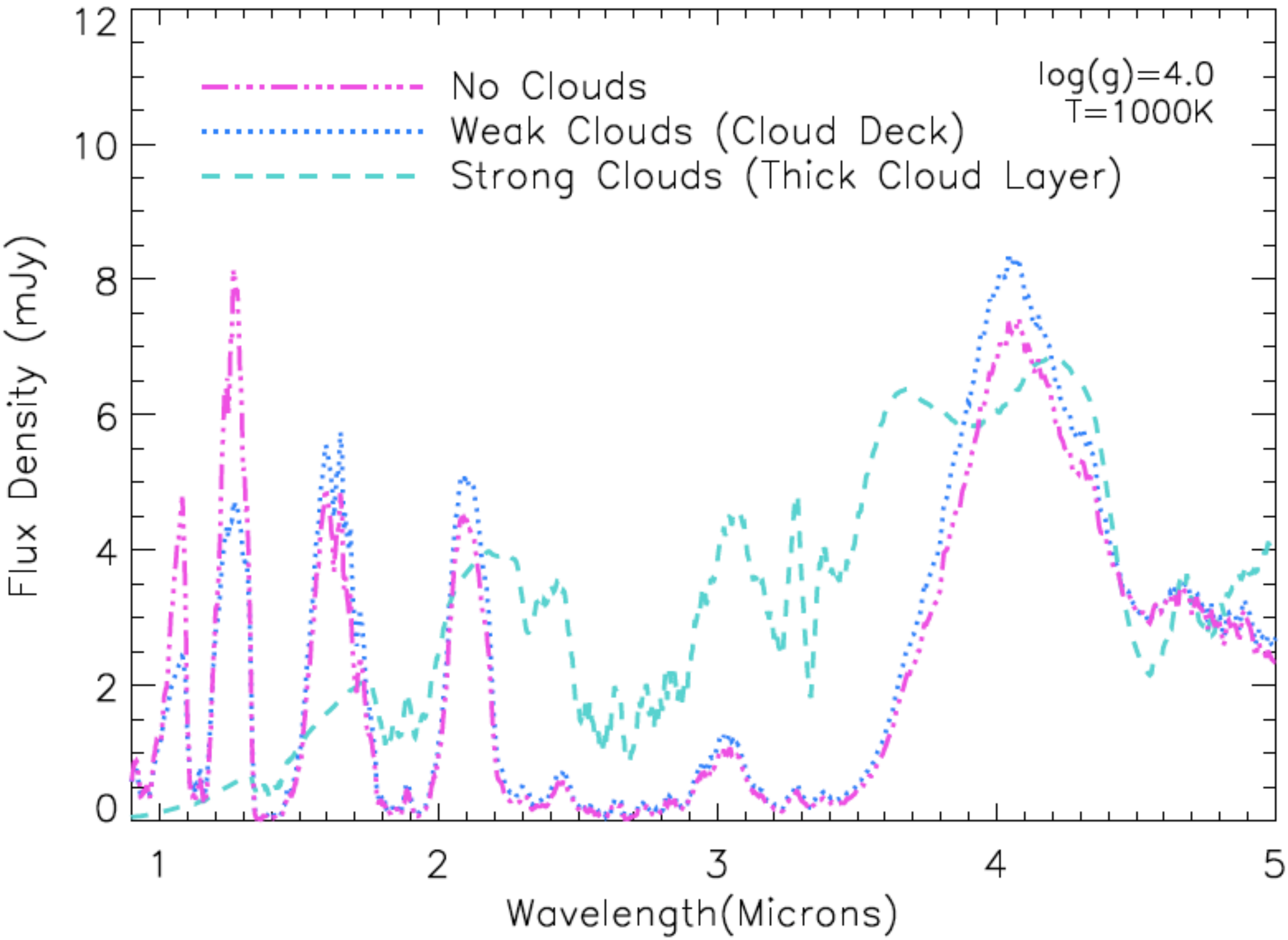
No Clouds
Weak Clouds (Cloud Deck)
Strong Clouds (Thick Cloud Layer)
log(g)=4.0
T=1000K
Flux Density (mJy)
Wavelength(Microns)
0
2
4
6
8
10
12
1
2
3
4
5

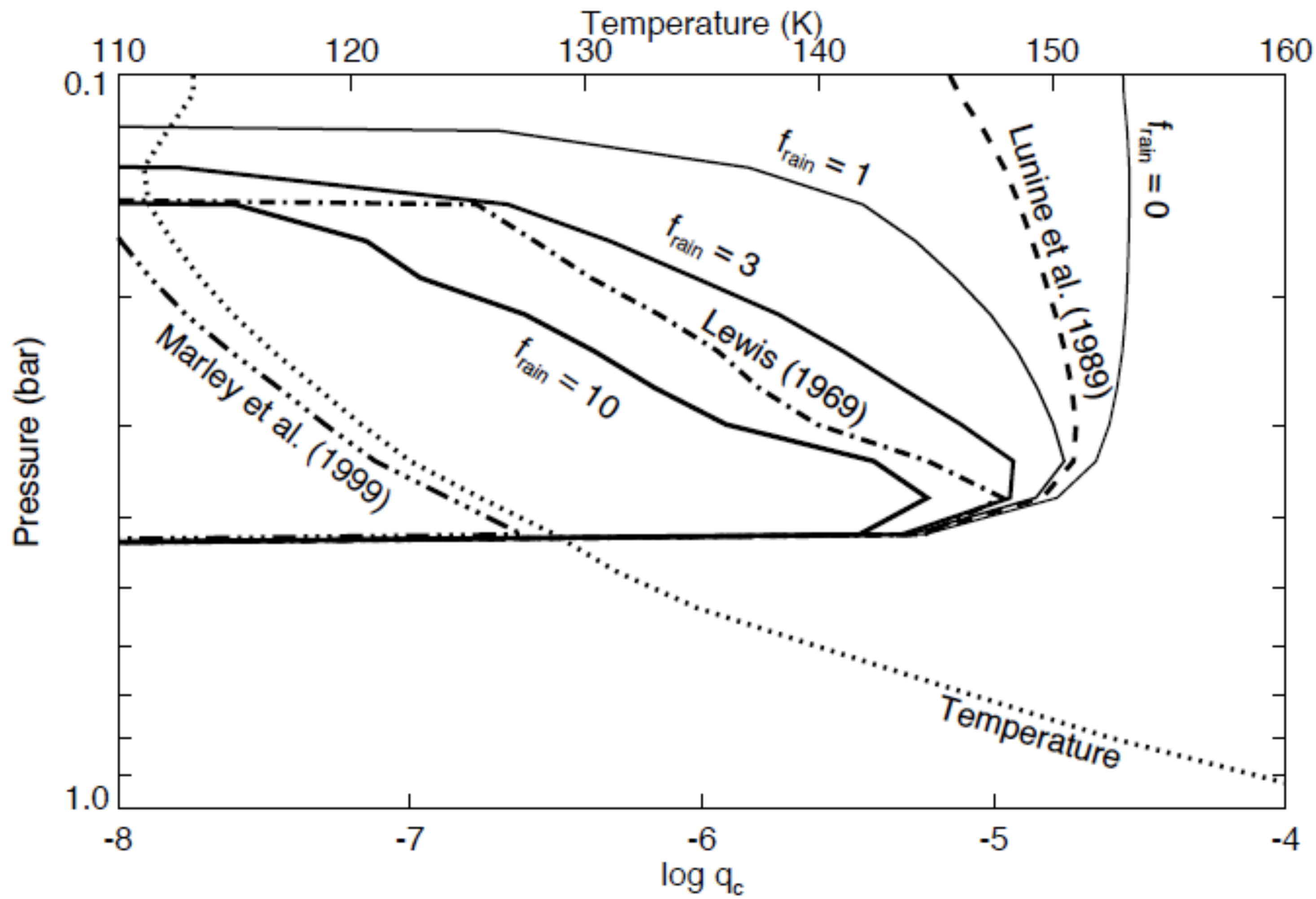

FIG. 1.—Vertical profiles of mole fraction (mixing ratio by volume) of condensed ammonia (q_c) from the present model of Jovian ammonia cloud with different values $f_{\rm rain}$ and from our adaptations of other models as labeled. The vertical coordinate is atmospheric pressure. The dotted line is the temperature profile. The kinks in the condensate profiles are caused by ripples in the temperature profile.

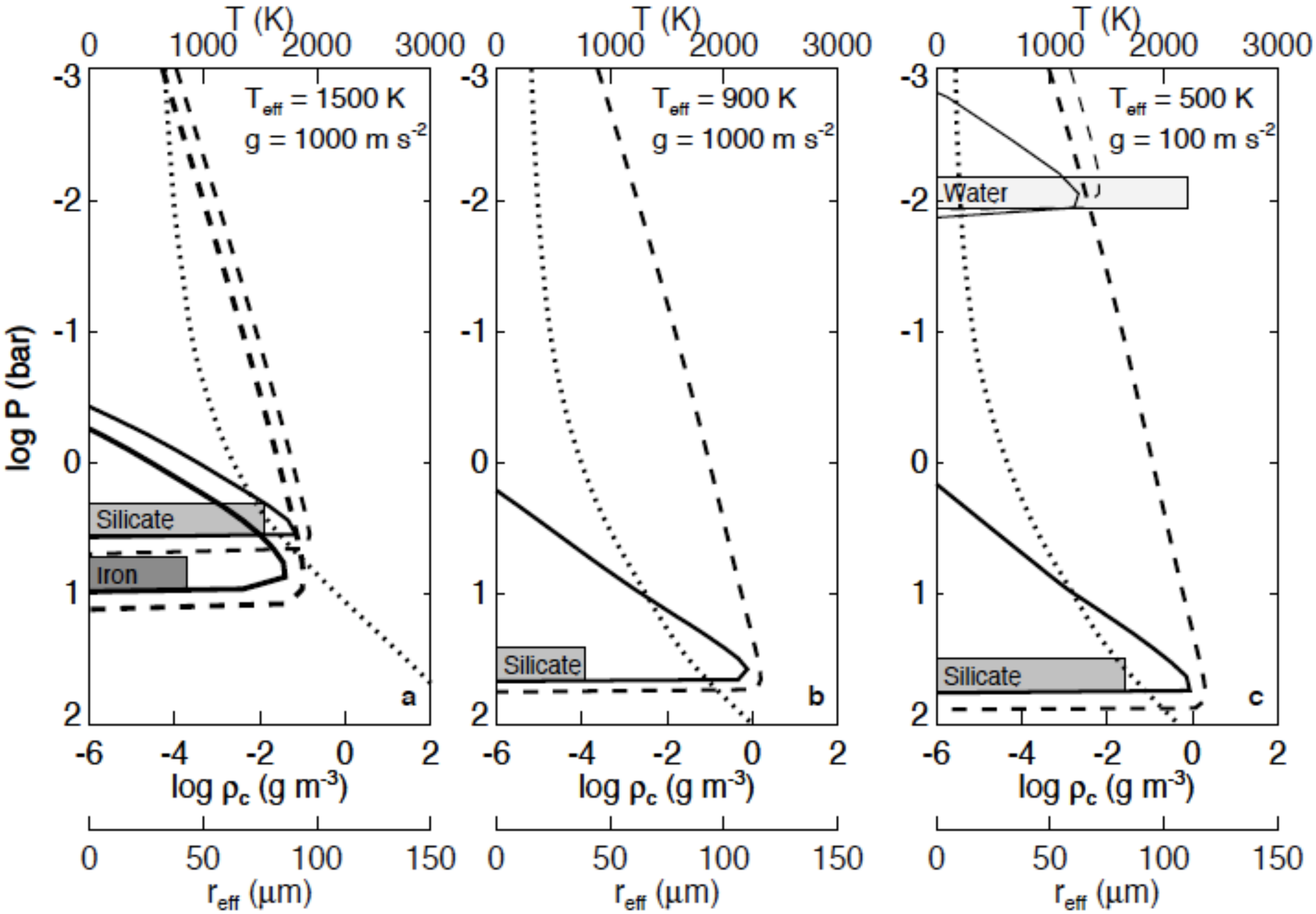

FIG. 6.—Profiles of temperature (*dotted curves*) and condensate mass concentration from baseline model (ρ_c, *solid curves*) in theoretical atmospheres of an (*a*) L dwarf, (*b*) T dwarf, and (*c*) extrasolar giant planet. Droplet effective radii at cloud base are shown as horizontal bars. Well-mixed clouds are shown as dashed curves. The theoretical temperature profiles are calculated for cloud-free conditions.

Ackerman & Marley (2001)

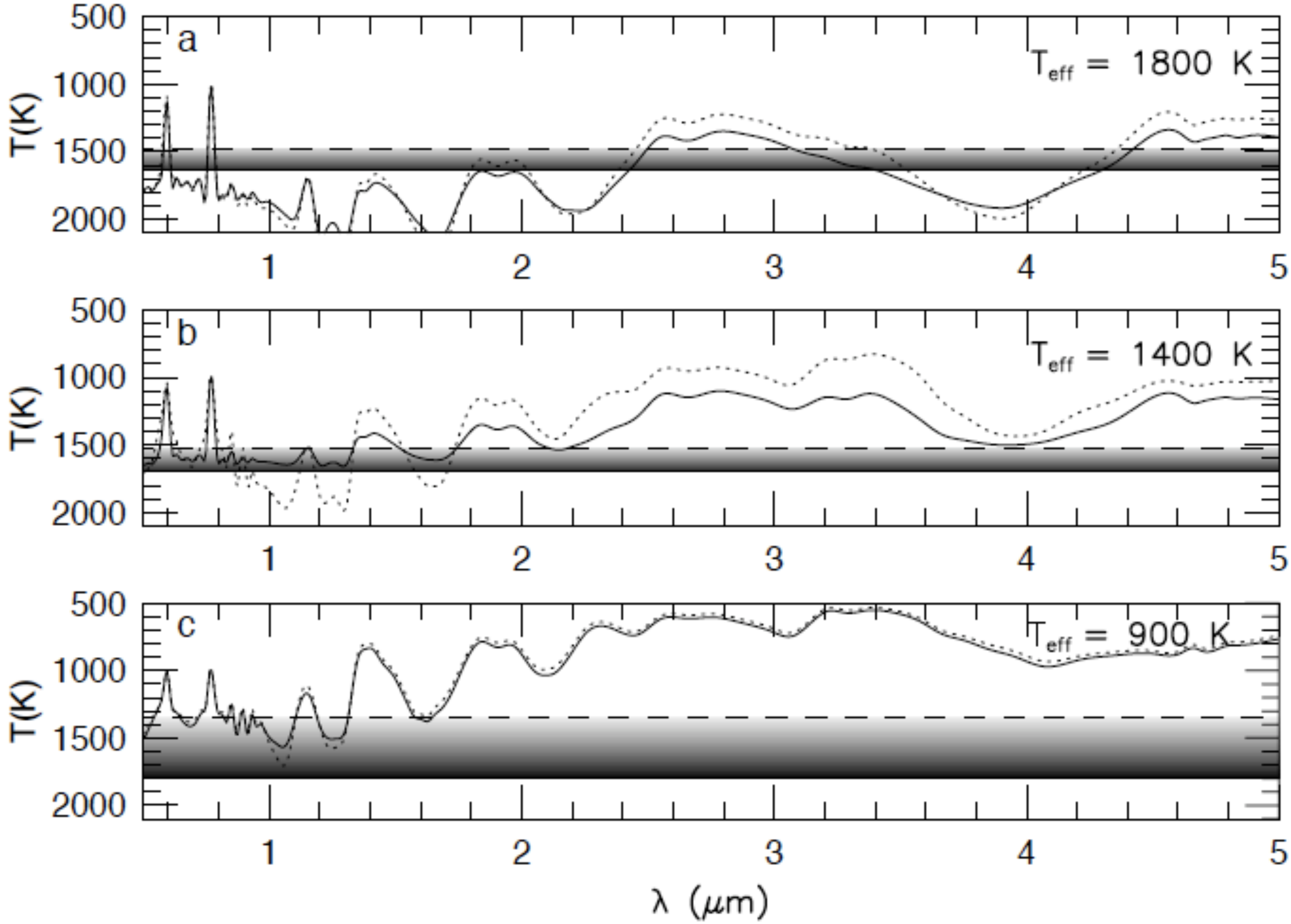

Ackerman & Marley (2001)

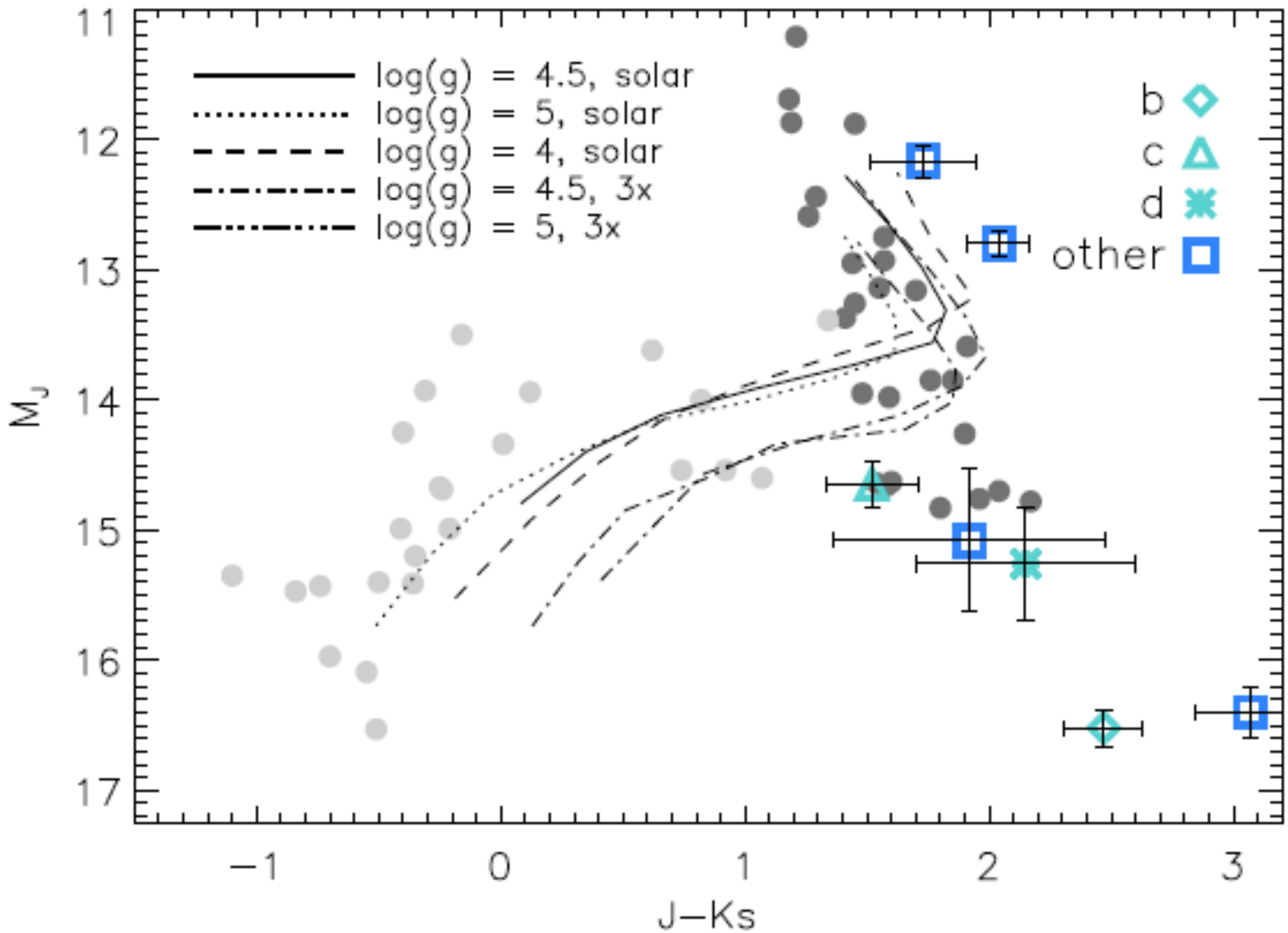

Currie et al. (2011)

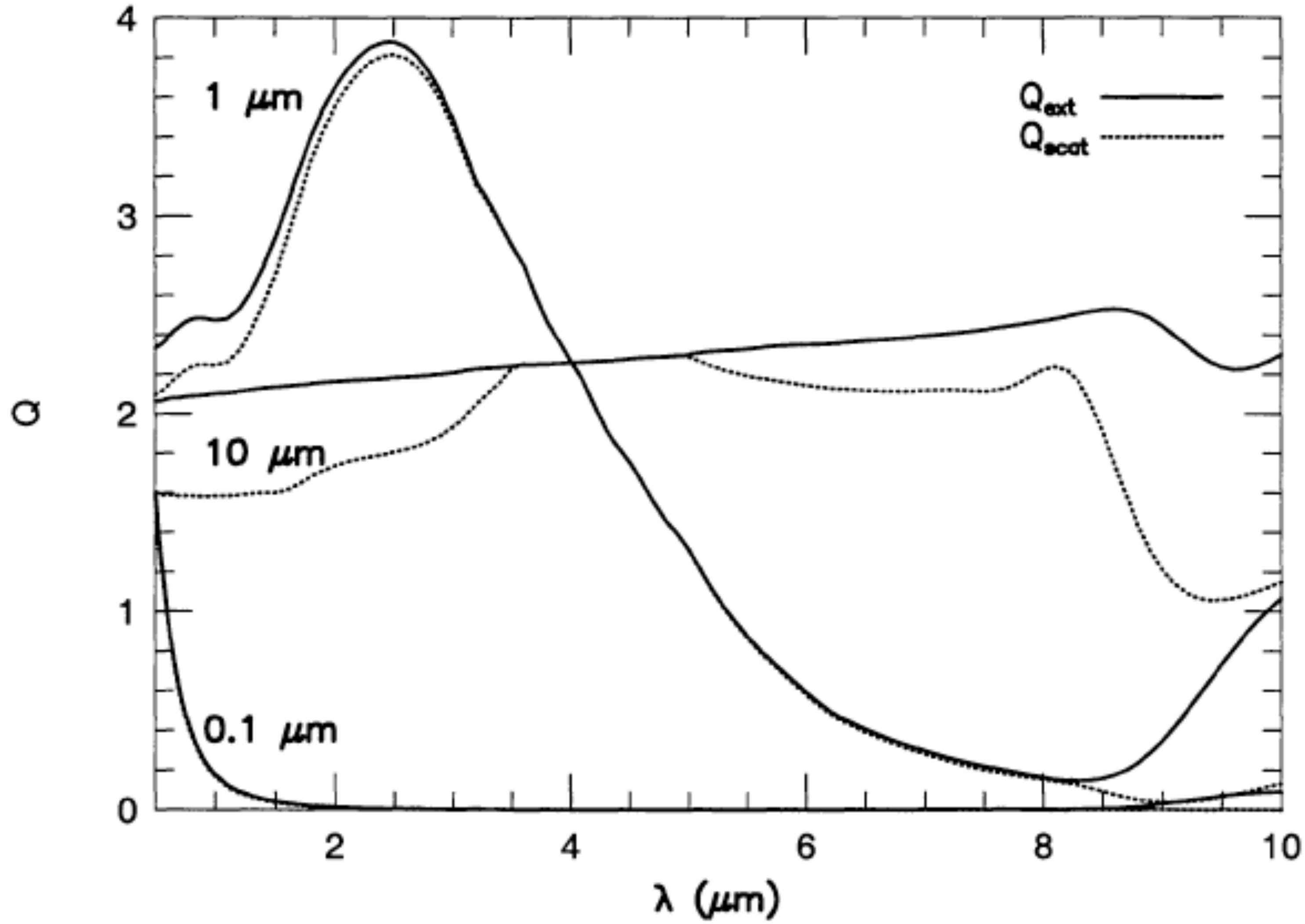

Figure 3. Mie extinction, $Q_{\rm ext}$, and scattering, $Q_{\rm scat}$, efficiencies for $MgSiO_3$ grains of various radii. Calculation assumes a size distribution similar to that found in some giant planet hazes (see Marley et al. 1999).

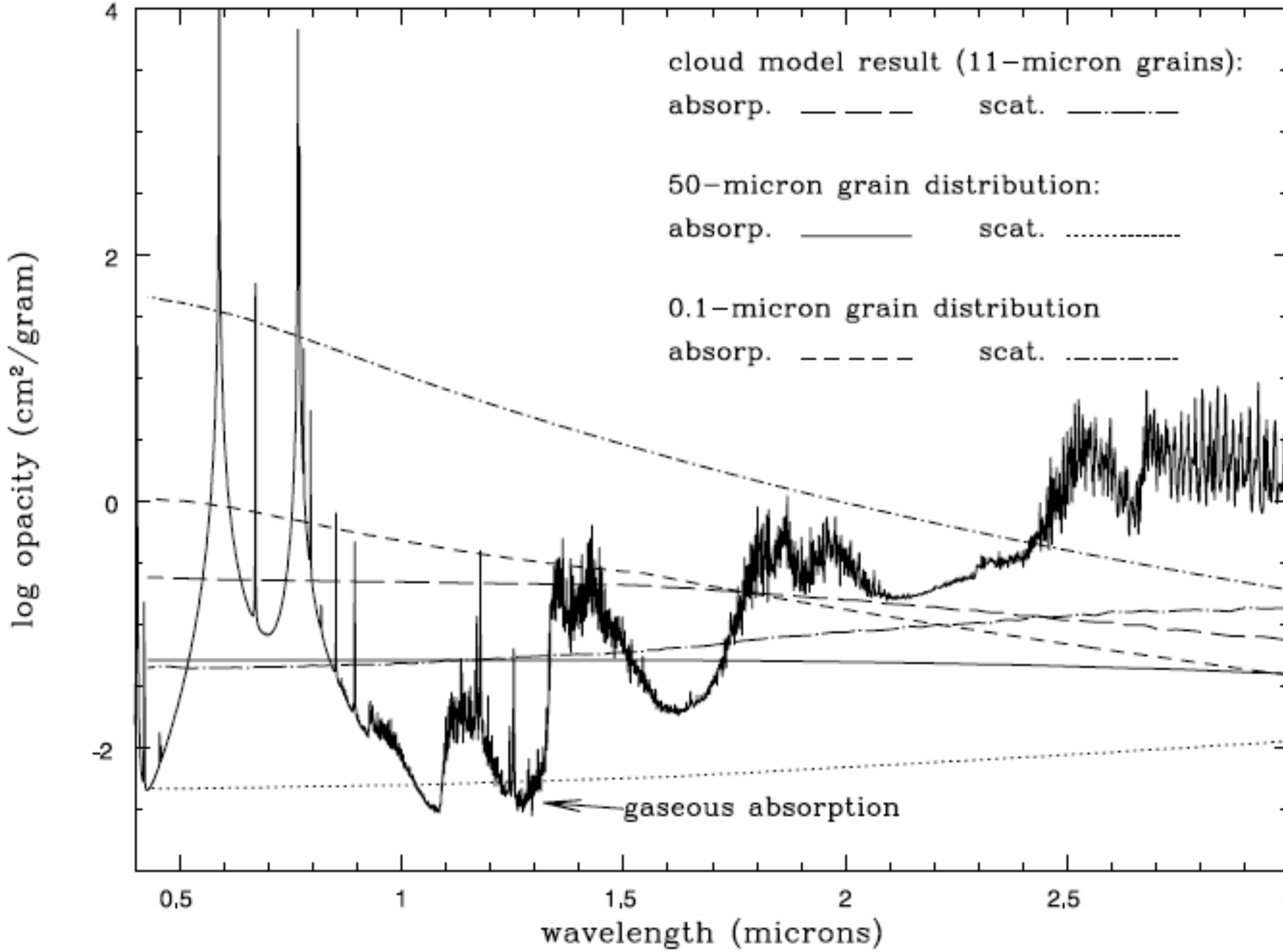

cloud model result (11−micron grains):
absorp.
scat.
50−micron grain distribution:
absorp.
scat.
0.1−micron grain distribution
absorp.
scat.
gaseous absorption
log opacity (cm²/gram)
4
2
0
-2
0,5
1
1,5
2
2,5
3
wavelength (microns)

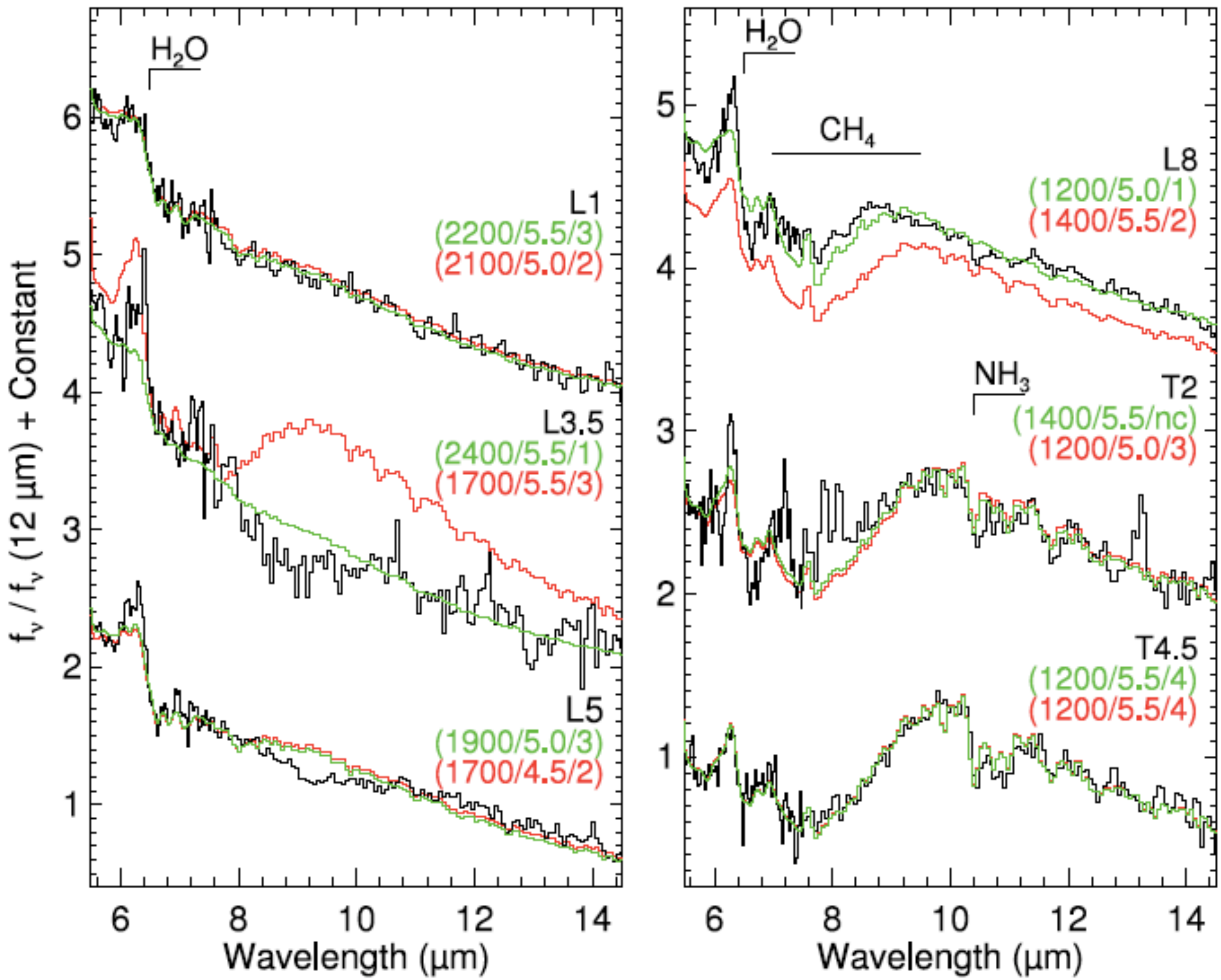

Fig. 18.—Same as Fig. 14, except the data cover the IRS/SL wavelength range and were normalized at 12 μm.

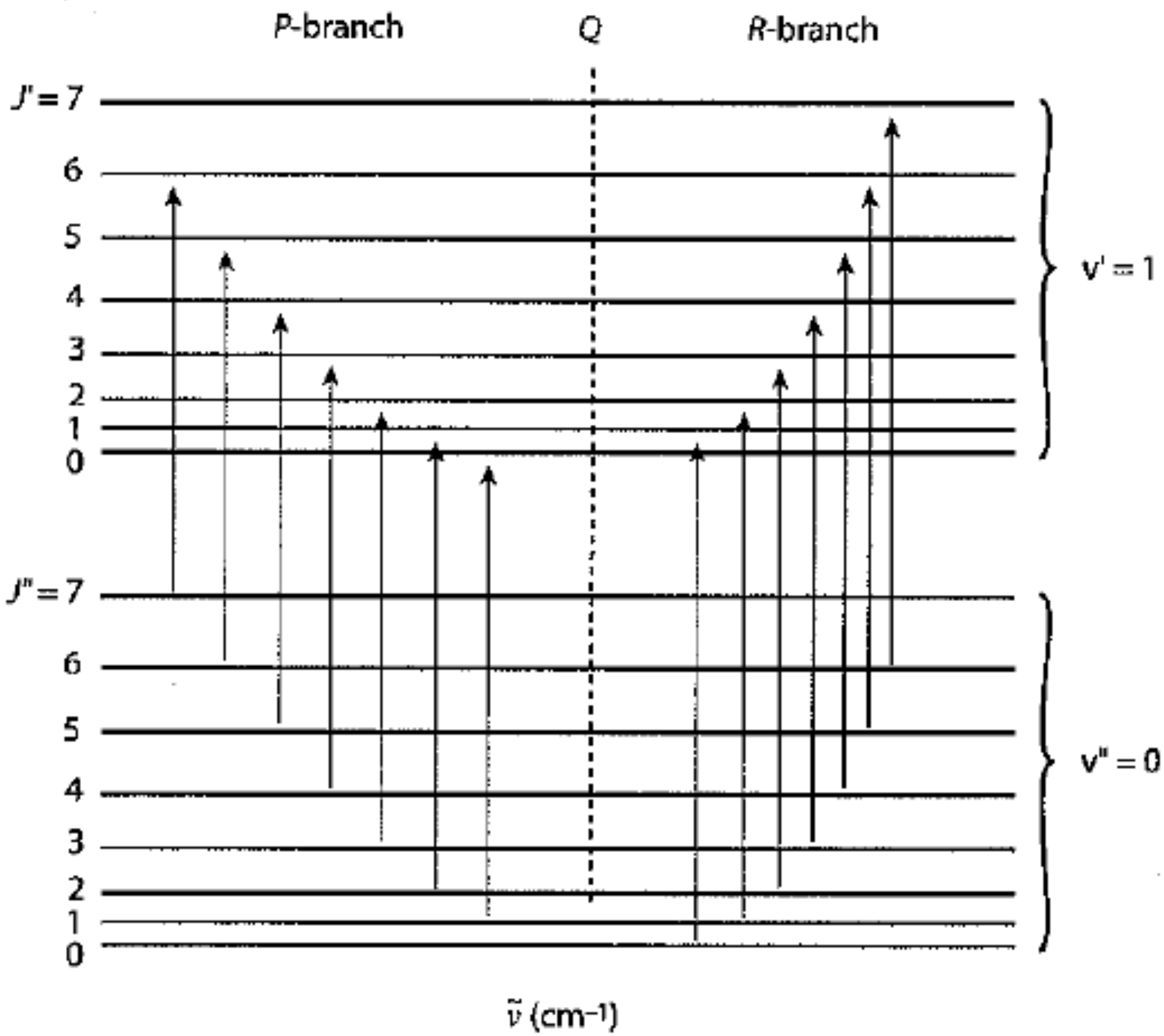

P-branch
Q
R-branch
J' = 7
6
5
4
3
2
1
0
v' = 1
J" = 7
6
5
4
3
2
1
0
v" = 0
$\tilde{\nu}$ (cm⁻¹)

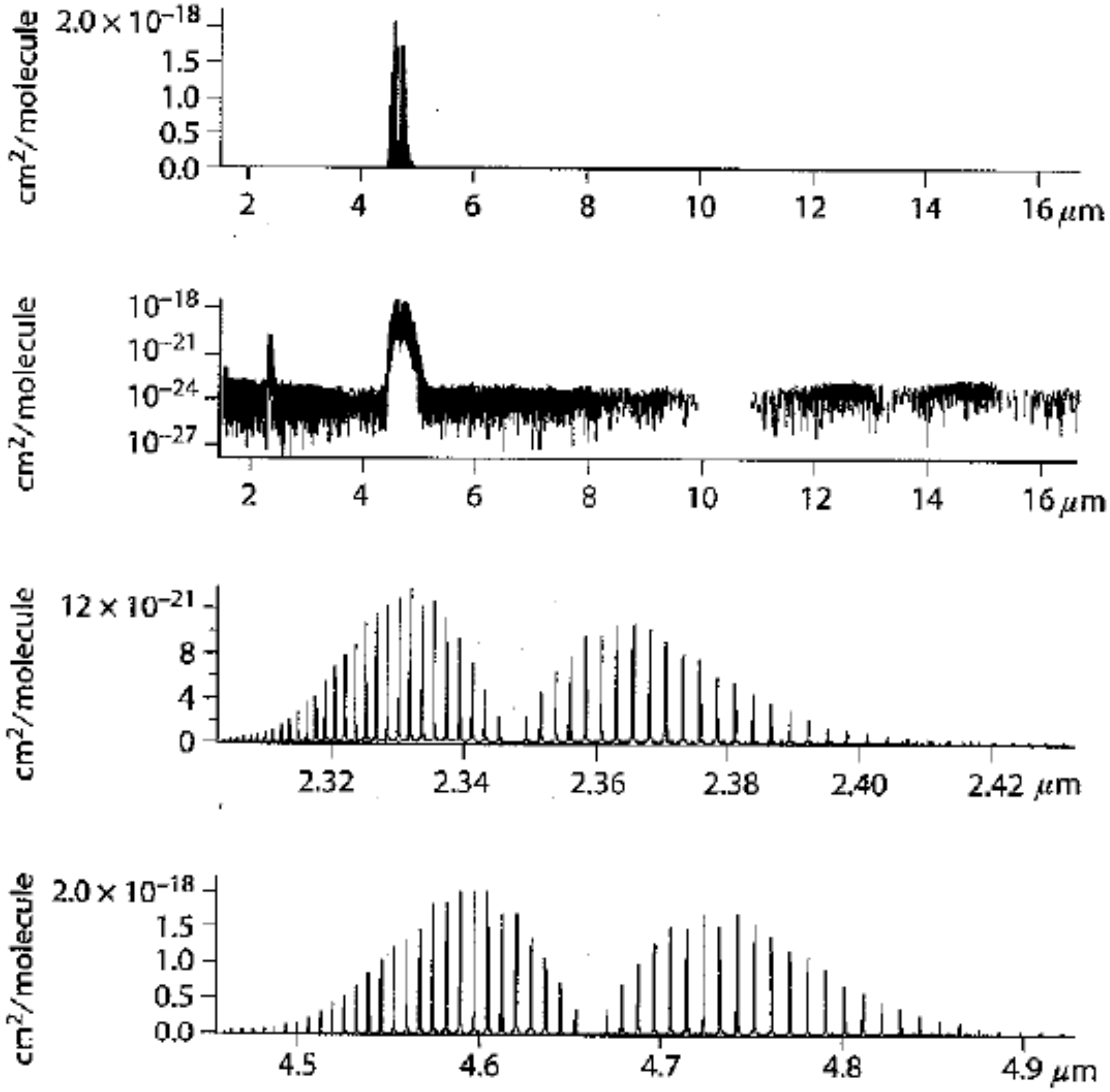

8.7 Simulated intensity of rotational-vibrational transitions of the CO molecule. The rotational transitions are centered around the P- and R-branches. The line intensities are approximately correct for a temperature of 300 K. The vibrational transition is the $v = 1 - 0$ band. Adapted from [6].

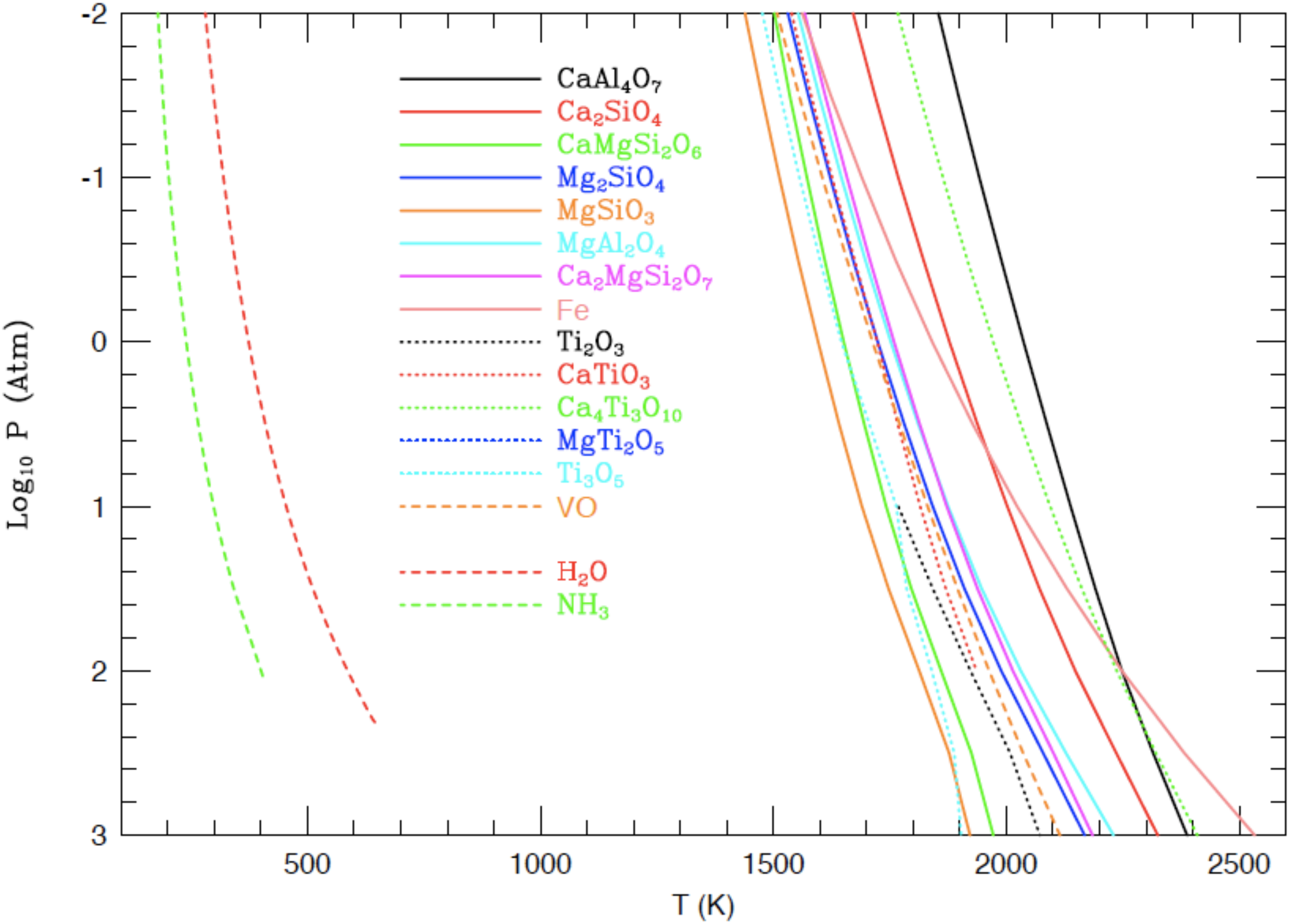

-2
-1
0
1
2
3
500
1000
1500
2000
2500
T (K)
Log10 P (Atm)
CaAl4O7
Ca2SiO4
CaMgSi2O6
Mg2SiO4
MgSiO3
MgAl2O4
Ca2MgSi2O7
Fe
Ti2O3
CaTiO3
Ca4Ti3O10
MgTi2O5
Ti3O5
VO
H2O
NH3

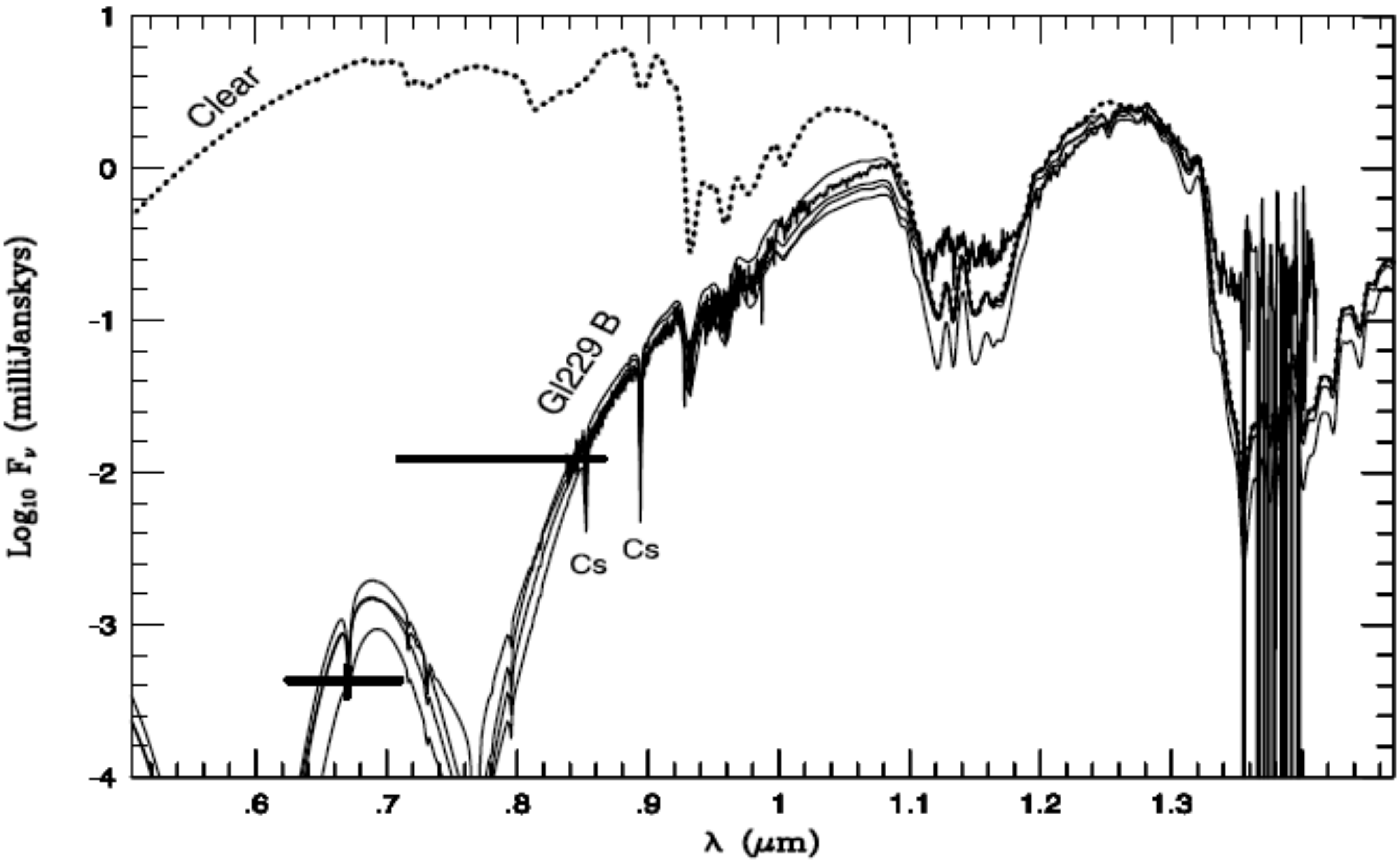

Burrows, Marley, & Sharp (2000)

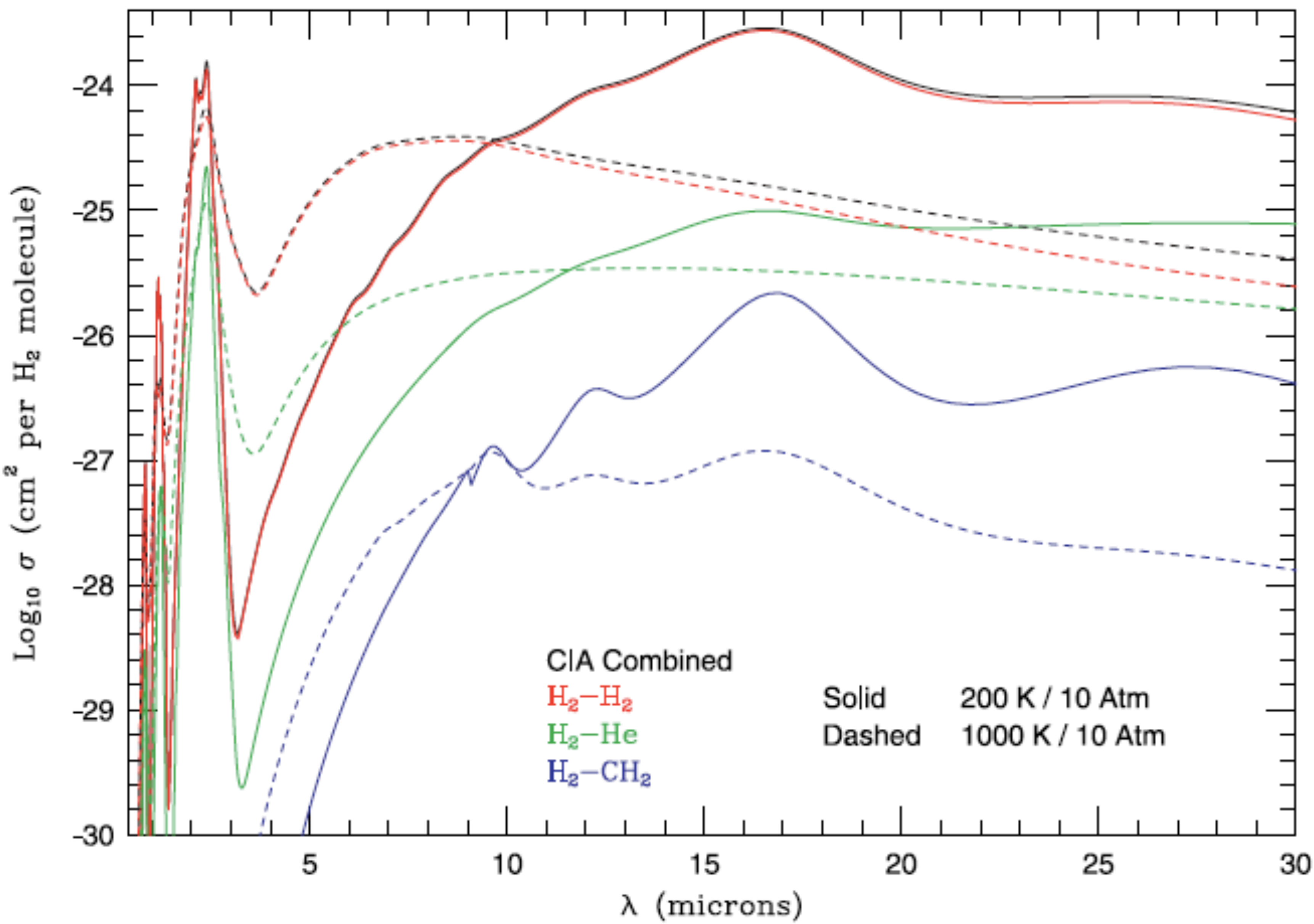

-24
-25
-26
-27
-28
-29
-30
5
10
15
20
25
30
Log10 σ (cm2 per H2 molecule)
λ (microns)
CIA Combined
H2−H2
H2−He
H2−CH2
Solid 200 K / 10 Atm
Dashed 1000 K / 10 Atm

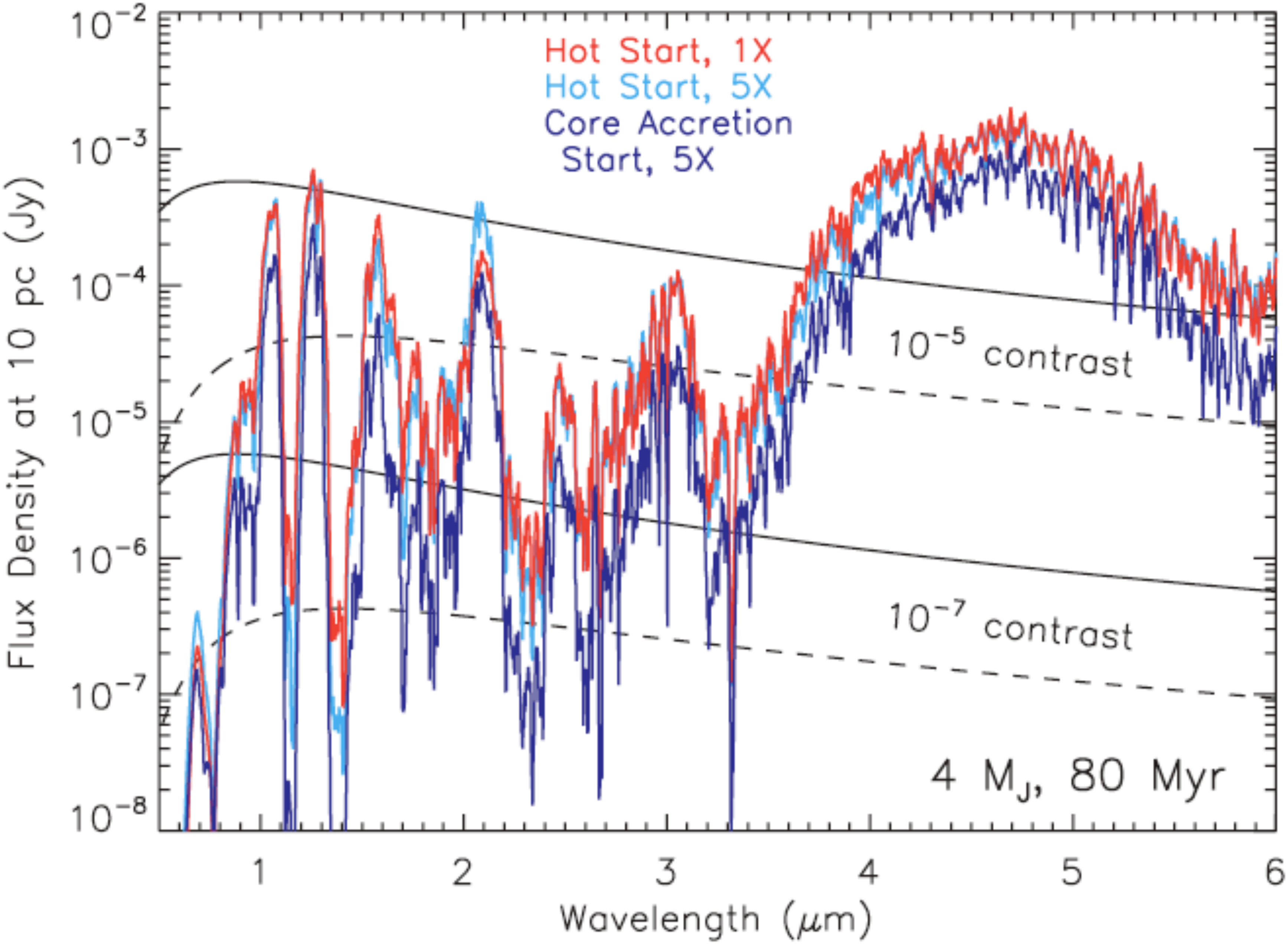

Hot Start, 1X
Hot Start, 5X
Core Accretion
Start, 5X
10^{-5} contrast
10^{-7} contrast
4 M_J, 80 Myr
Flux Density at 10 pc (Jy)
Wavelength (μm)
10^{-2}
10^{-3}
10^{-4}
10^{-5}
10^{-6}
10^{-7}
10^{-8}
1
2
3
4
5
6

Fortney et al. (2008)

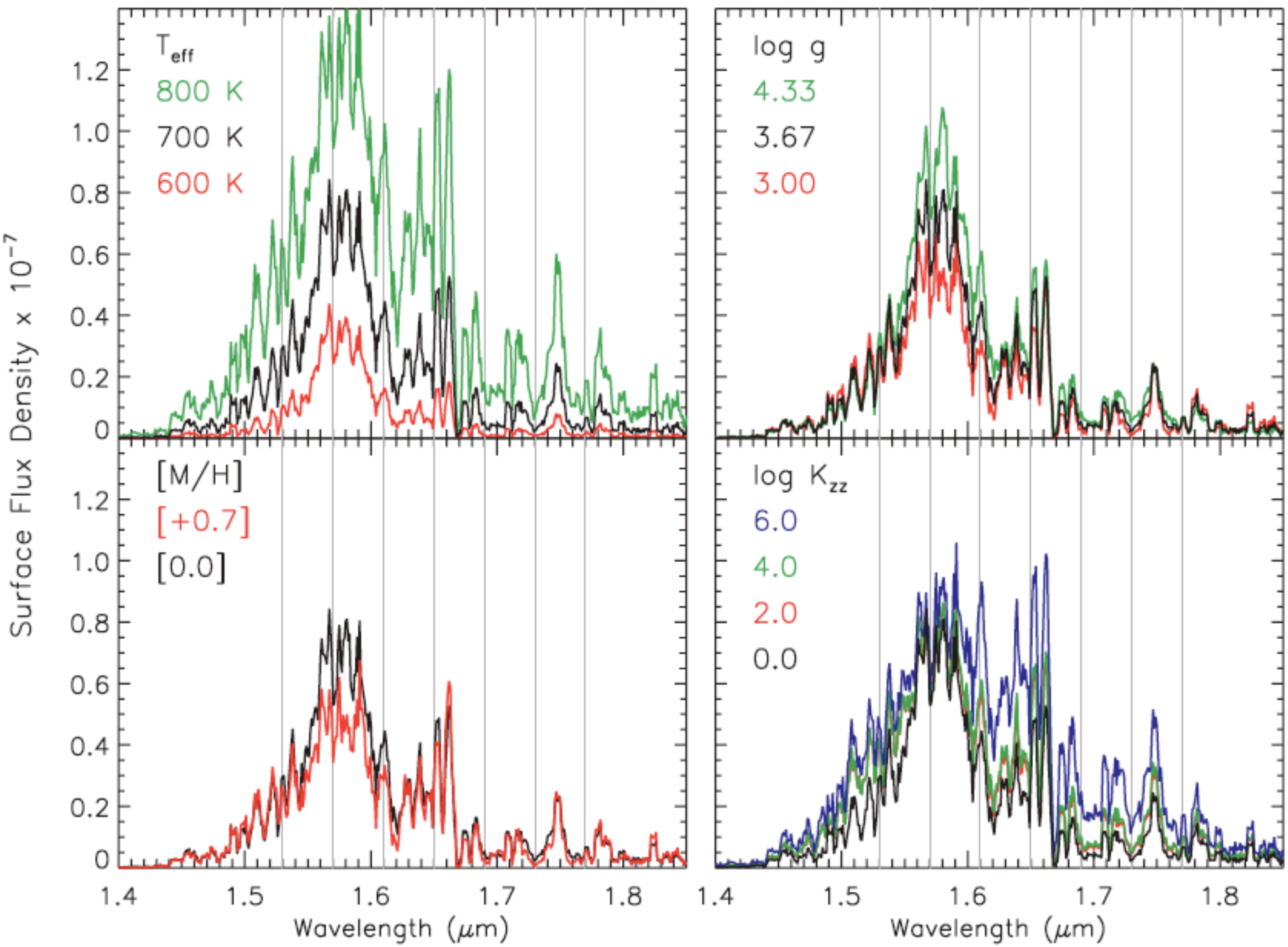

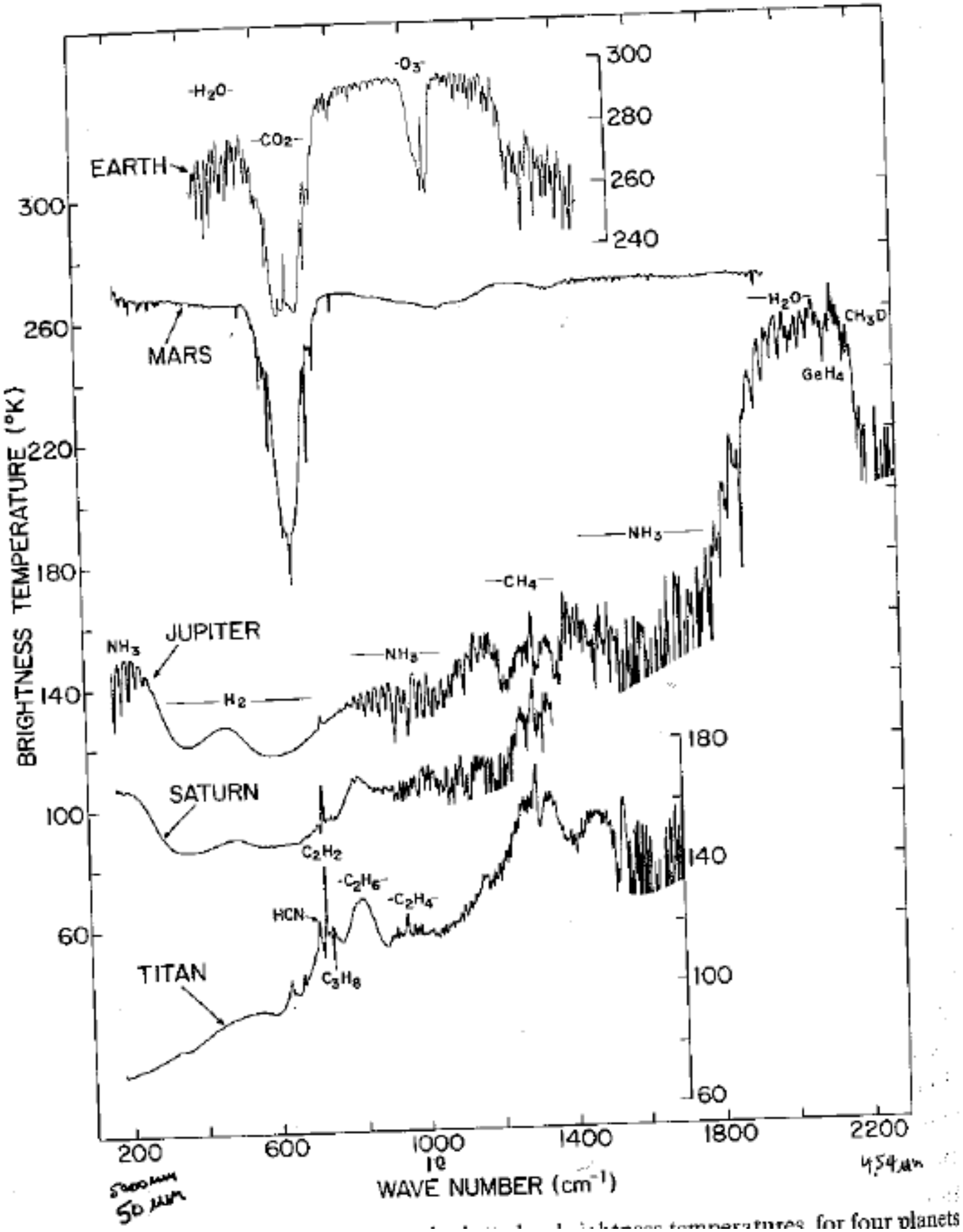

... brightness temperatures for four planets

Galileo Entry Probe, 1995

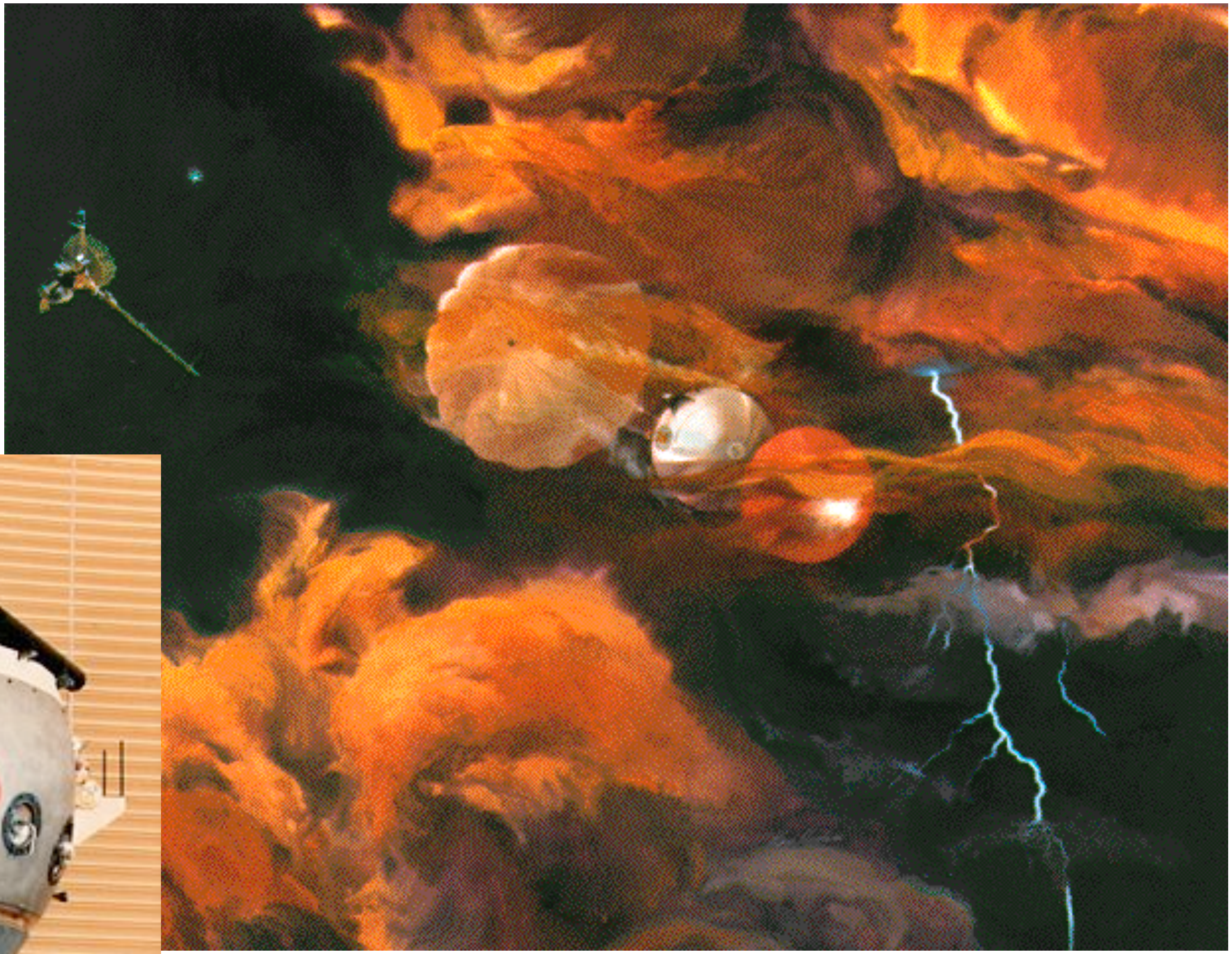

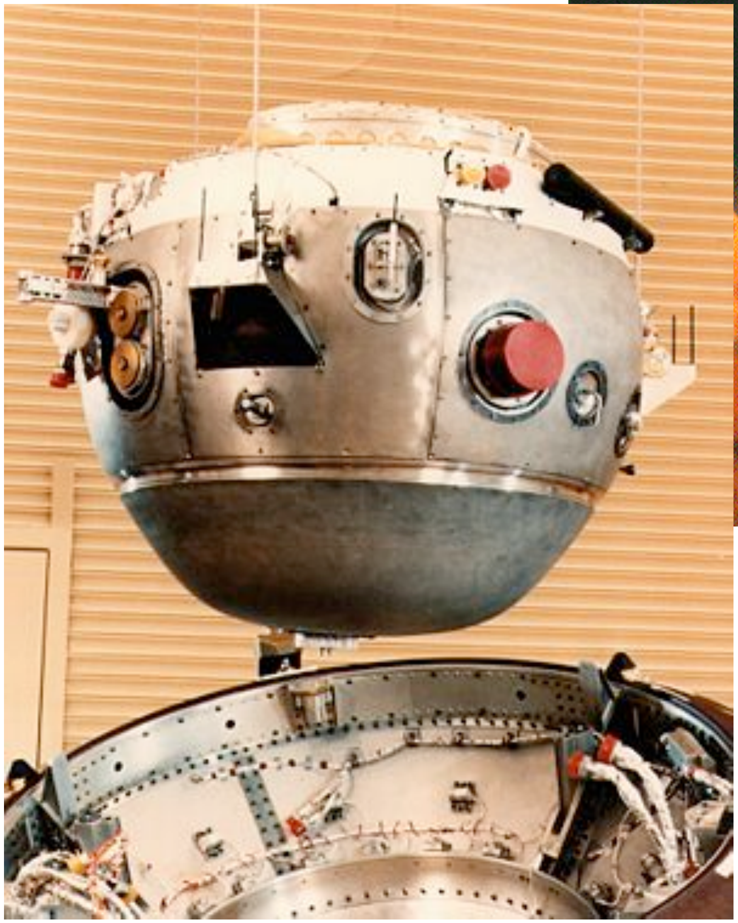

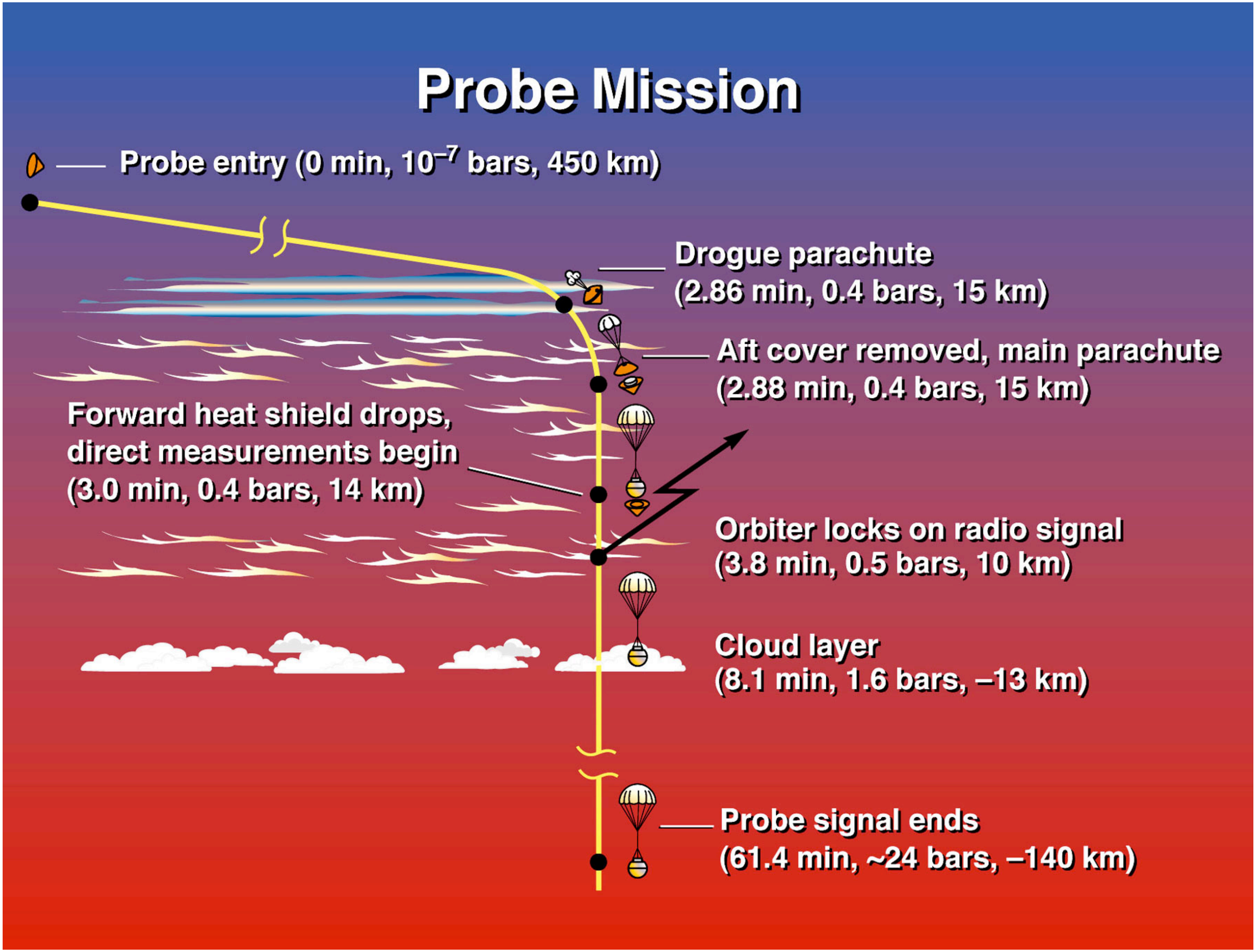

Probe Mission
Probe entry (0 min, 10–7 bars, 450 km)
Drogue parachute
(2.86 min, 0.4 bars, 15 km)
Aft cover removed, main parachute
(2.88 min, 0.4 bars, 15 km)
Forward heat shield drops,
direct measurements begin
(3.0 min, 0.4 bars, 14 km)
Orbiter locks on radio signal
(3.8 min, 0.5 bars, 10 km)
Cloud layer
(8.1 min, 1.6 bars, –13 km)
Probe signal ends
(61.4 min, ~24 bars, –140 km)

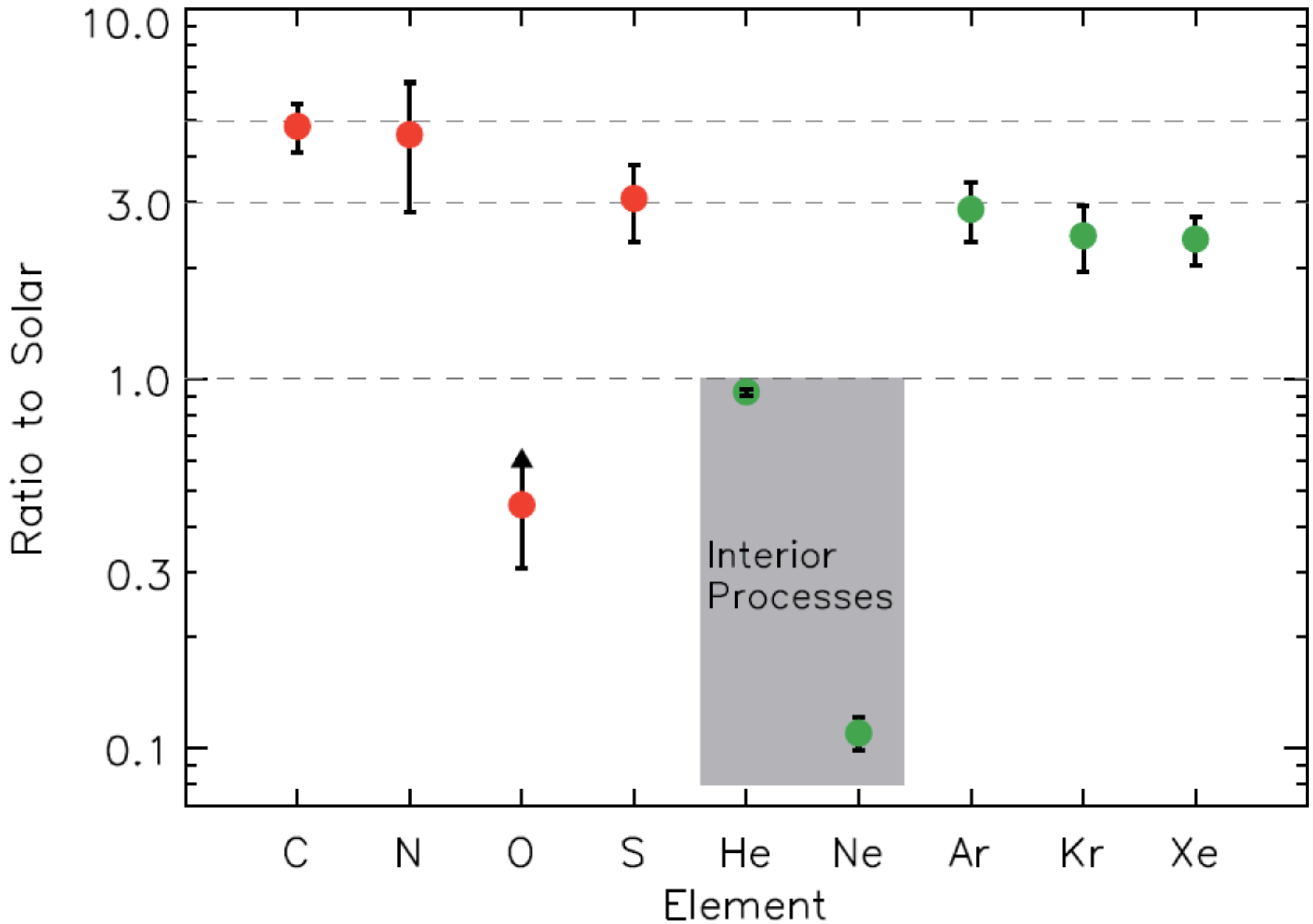

10.0
3.0
1.0
0.3
0.1
Ratio to Solar
Interior Processes
C
N
O
S
He
Ne
Ar
Kr
Xe
Element

Guillot (2005)

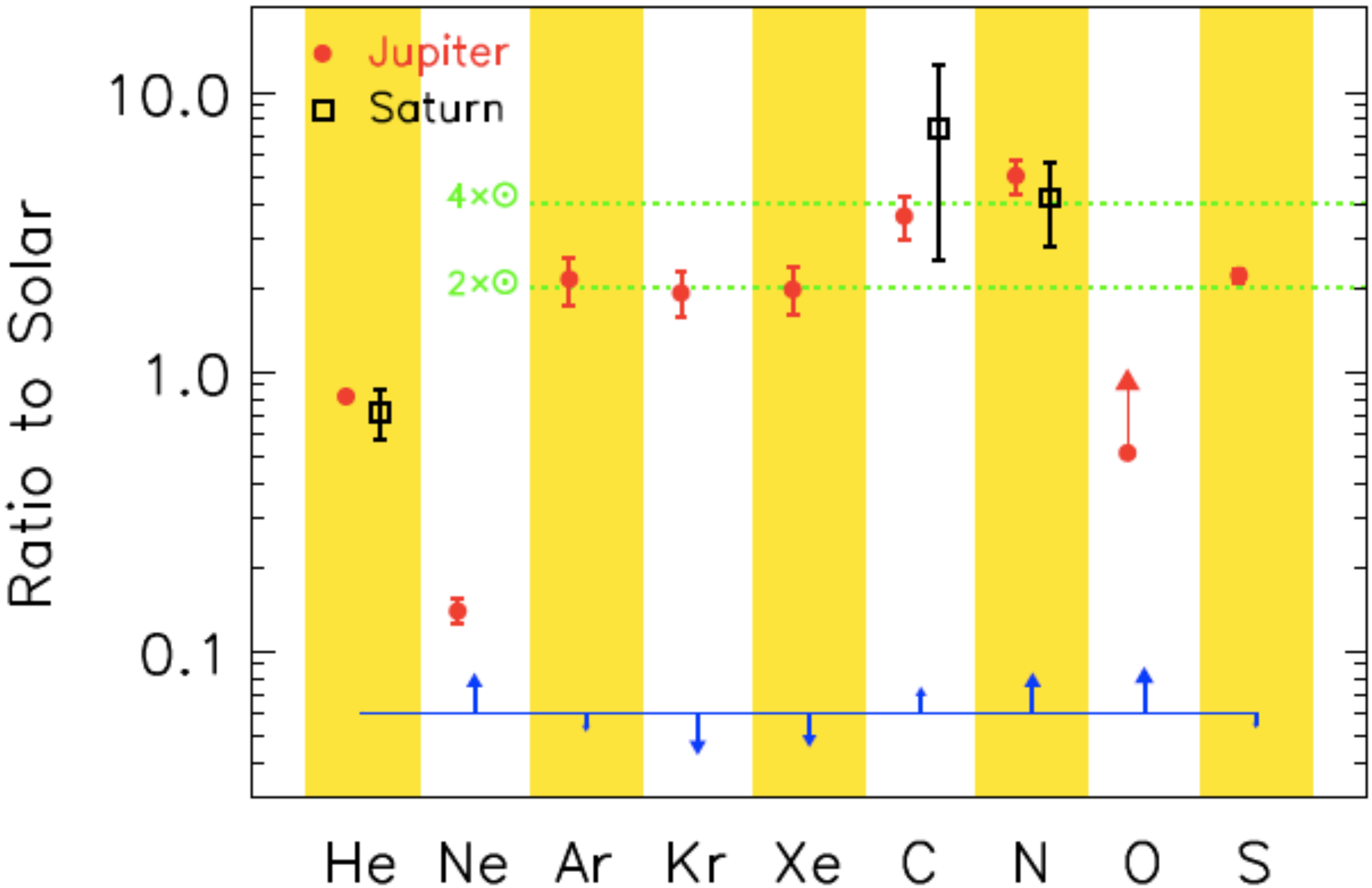

Abundance Ratios in the Giant Planets.

Ratio	J/Sun	S/Sun	U/Sun	N/Sun
C/H	2.9 ± 0.5 [a)]	$6.1^{+3.3}_{-2.6}$ [b)]	23^{+10}_{-7} [c)]	31^{+7}_{-8} [c)]
N/H	3.3 ± 1.5 [d)] (P=9-12 bar)	2-4 [e)]		
O/H	2.4×10^{-4} [a)] (P=3.6 bar)	2×10^{-4} [f)] (P=3-5 bar)		
	0.033 ± 0.015 [g)] (P=12 bar)			
	$0.35^{+0.23}_{-0.16}$ [g)] (P=19 bar)			
P/H	0.75 ± 0.25 [h)] (P=1-2 bar)	3 ± 1.5 [i)]		
S/H	2.5 ± 0.15 [a)] (P>16 bar)			
He/H*	0.807 [j)]	0.56-0.85 [k)]	0.9 [j)]	1.2 [j)]
Ne/H	0.10 ± 0.01 [a)]			
Ar/H	2.5 ± 0.5 [l)]			
Kr/H	2.7 ± 0.5 [l)]			
Xe/H	2.6 ± 0.5 [l)]			

[a)] GPMS, Niemann *et al.* (1998); [b)] Voyager 7.7 μm, Courtin *et al.* (1984);
[c)] GB visible and NIR, Baines *et al.* (1995); [d)] GPMS, Atreya *et al.* (2002);
[e)] GB IR and radio, Marten *et al.* (1980); de Pater and Massie (1985);
[f)] ISO 5 μm, de Graauw *et al.* (1997); [g)] GPMS, Atreya *et al.* (1999); Wong *et al.* (2002a);
[h)] Voyager 5 μm, Drossart *et al.* (1982);
[i)] Voyager 10 μm, Courtin *et al.* (1984); GB submm, Weisstein and Serabyn (1994);
[j)] after von Zahn *et al.* (1998); [k)] after Conrath and Gautier (2000); [l)] Mahaffy *et al.* (2000);
* relative to the protosolar value of He/H.

A low-temperature origin for the planetesimals that formed Jupiter

Tobias Owen*, Paul Mahaffy†, H. B. Niemann†, Sushil Atreya‡, Thomas Donahue‡, Akiva Bar-Nun§ & Imke de Pater‖

ENRICHMENTS IN VOLATILES IN JUPITER: A NEW INTERPRETATION OF THE *GALILEO* MEASUREMENTS

D. Gautier, F. Hersant,[1,2] and O. Mousis[3]
DESPA/Observatoire de Meudon, CNRS-UMR 8632, F-92195 Meudon, France; daniel.gautier@obspm.fr
and
J. I. Lunine
Lunar and Planetary Laboratory, University of Arizona, Space Sciences Building, P.O. Box 210092, Tucson, AZ 85721
Received 2001 January 8; accepted 2001 February 21; published 2001 March 21

Deep H_2O and NH_3 abundances, at 100 bar, below the clouds